Advances in Nano Research, *Vol. 9, No. 3 (2020) 133-145*
DOI: https://doi.org/10.12989/anr.2020.9.3.133

A study on the dynamic instabilities of a smart embedded micro-shell induced by a pulsating flow: A nonlocal piezoelastic approach

Vahid Atabakhshian* and Alireza Shooshtari[a]

Department of Mechanical Engineering, Faculty of Engineering, Bu-Ali Sina University, Hamedan, I.R., Iran

(*Received January 30, 2018, Revised May 29, 2018, Accepted April 14, 2020*)

Abstract. In this study, nonlinear vibrations and dynamic instabilities of a smart embedded micro shell conveying varied fluid flow and subjected to the combined electro-thermo-mechanical loadings are investigated. With the aim of designing new hydraulic sensors and actuators, the piezoelectric materials are employed for the body and the effects of applying electric field on the stability of the system as well as the induced voltage due to the dynamic behavior of the system are studied. The nonlocal piezoelasticity theory and the nonlinear cylindrical shell model in conjunction with the energy approach are utilized to mathematically modeling of the structure. The fluid flow is assumed to be isentropic, incompressible and fully develop, and for more generality of the problem both steady and time dependent flow regimes are considered. The mathematical modeling of fluid flow is also carried out based on a scalar potential function, time mean Navier-Stokes equations and the theory of slip boundary condition. Employing the modified Lagrange equations for open systems, the nonlinear coupled governing equations of motion are achieved and solved via the state space problem; forth order numerical integration and Bolotin's method. In the numerical results, a comprehensive discussion is made on the dynamical instabilities of the system (such as divergence, flutter and parametric resonance). We found that applying positive electric potential field will improve the stability of the system as an actuator or vibration amplitude controller in the micro electro mechanical systems.

Keywords: parametric instability; time dependent flow; smart materials; Bolotin's method; small scale parameter

1. Introduction

It is well accepted among researchers that the nanotechnology will be the basis of the future industrial revolution and the discovery of nanotubes is one of the major advances in this regard. Generally, nanotechnology involves construction and application of biological, chemical and physical systems ranging from micro to nanometer. Nowadays, the micro and nanotubes conveying fluid have been an area of active researches due to their extensive possible applications in biological systems (e.g., biological separation, biosensing, molecular imaging), medicine (e.g., drug delivery), chemistry (e.g., fuel storing cells, chemical analyses), physics (e.g., optical structures) and other research areas (Gao and Xu 2009, Kong *et al*. 2000, Dharap *et al*. 2004).

The dynamic and instability analyses of a fluid conveying pipe is one of the important challenges in the field of fluid conveying systems which were basically considered in 1950 on the Trans-Arabian pipeline project (Ashley and Haviland 1950). Certainly, the vast applications of pipes conveying or containing fluids in various industries such as in oil and gas, water and sewage, military and aerospace, medical and chemistry is enough to attract more considerations of the researchers in this regard. Following some of the valuable pioneering works.

Paidoussis (1998) examined the fluid and body interactions in slender structures conveying axial flows. He modeled and analyzed the dynamics and instabilities of fluid conveying systems. Amabili (2008) also studied the nonlinear dynamics and instabilities of circular cylindrical shells conveying fluid and classified the fluid instabilities for circular cylindrical shells conveying fluid. He utilized various nonlinear shell models, modal expansion analyses and energy approaches to present a comprehensive analysis about the problem. Dynamical behavior of the fluid conveying pipes based on various types of beam theories is investigated by Reddy and Wang (2004). They obtained equation of motion via energy approaches where employed finite element method to solve the problem. Pellicano and Amabili (2006) studied dynamics and instabilities of empty and fluid filled circular cylindrical shells under external loadings. They used modal analyses approach to simulate the problem. Sadeghi and Karimi-Dona (2011) employ a FEM-state space approach beside MATLAB program to modeling the dynamical behaviors of fluid conveyed pipes with a sprung mass moving on it. Gu *et al*. (2016) used integral transform technic to obtain the dynamical response of fluid conveying pipes.

In the micro and nano scale problems and in the field of biomechanics the flutter phenomenon of veins conveying blood flow is investigated by Kamm (1989). Paidoussis (2003) proposed a model for the fluid-structure interaction between the blood flow and veins. Moreover, in the field of

*Corresponding author, Ph.D.,
E-mail: V.atabakhshian@gmail.com
[a] Ph.D., E-mail: shooshta@basu.ac.ir

ISSN: 2287-237X (Print), 2287-2388 (Online)

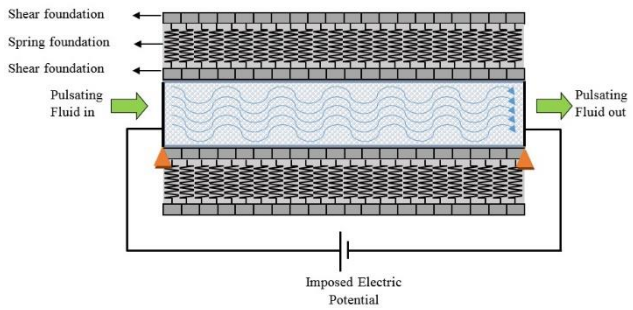

Fig. 1 Schematic of embedded smart micro-shell conveying pulsating fluid

nano mechanic, Yan *et al*. (2009) studied the stability and critical flow velocity of multi-walled carbon nanotubes (CNTs) conveying fluid. Nonlinear vibration analysis of double walled CNTs conveying fluid is carried out by Kuang *et al*. (2009). Arani *et al*. (2013a) studied Flow induced vibration and instability of a smart polymeric micro tube subjected to the axial electric field. They obtained that imposing electric potential field has a significant effect on the stability of the smart micro tube. In another work Arani *et al*. (2013b) studied nonlinear dynamical response of embedded fluid-conveyed micro-tubes reinforced by BNNTs. Atabakhshian *et al*. (2015) studied nonlinear dynamics and instability of a an elastically coupled CNT-PPB system with internal flow. They purpose a novel active control approach for instability of CNTs conveying steady fluid flow.

In all of the above investigations, a steady flow velocity is considered inside the structure which is not suitable for a lot of empirical problems like those with pumps or turbines in the pipelines. In this regard nonlinear dynamics of pipes conveying pulsating fluid with combination of parametric and internal resonances is studied by Panda and Kar (2008). Azrar *et al*. (2015) studied the dynamic and parametric instabilities of single-walled CNTs conveying pulsating and viscous fluid. Liang and Su (2013) utilized the averaging method for the stability analyses of a single-walled carbon nanotubes conveying pulsating and viscous fluid. Pipes conveying pulsating fluid and exposed on the external vortex is analyzed by Da *et al*. (2014). They employed multiple time scale method to obtain the parametric resonances of the system. Nonlinear dynamics of simply supported pipes with motion constraints and internal pulsating fluid is investigated by Wang (2009). Recently, micro pulsating fluid flow in heat pipes with alternate widths is examined by Yang *et al*. (2015). Tubaldi *et al*. (2016) modeled nonlinear dynamics of shells subjected to pulsating fluid flow. They utilized a special pulsatile time dependent function for blood flow velocity based on the heart beating period. They also recently examined in another work (Tubaldi *et al*. 2017), the effects of pulse-wave propagation on nonlinear dynamics of shell conveying pulsatile flow.

Based on the above survey, lack of proper research to instability prediction as well as instability smart control of Fluid conveying microtubes can be clearly felt. Hence, in this study, we investigate flow induced vibrations and instabilities of a smart embedded micro-shell conveying pulsating fluid as schematically is shown in Fig. 1. Parametric excitation due to harmonic pulsation in the flow velocity, Knudsen number effects, pulsation viscose effects, small scale parameter, Winkler and Pasternak modules and combined electro-mechanical loadings are taken into accounts. The unsteady fluid motion and the effect of viscosity for turbulent flow are modeled using potential flow theory and unsteady time-averaged Navier-Stokes equations, respectively. The governing equations of motion are derived using modal expansion analyses and the modified Lagrangian approach for open systems. In the results section, divergence, flutter and parametric resonance instabilities are examined in details. It is concluded that imposing axial electric field may be used as a controlling factor to improve the stability of the system. The results obtained in this study can specially utilized to design and manufacturing nano/micro electro-mechanical systems in advanced biomechanics applications with electrical fields as in hydrolic sensors and actuators.

2. Constitutive equations

2.1 Piezoelasticity theory

Based on piezoelasticity theory, stresses $\{\sigma\}$ and strains $\{\varepsilon\}$ as well as electric displacement $\{D\}$ and electric field $\{E\}$ vectors in piezoelectric materials may be combined as follows (IEEE Standard 1978)

$$\begin{Bmatrix}\sigma\\ D\end{Bmatrix}=\begin{bmatrix}C & -e\\ e^T & \in\end{bmatrix}\begin{Bmatrix}\varepsilon\\ E\end{Bmatrix}-\begin{Bmatrix}\lambda\\ p\end{Bmatrix}\Delta\Theta \tag{1}$$

where the coefficients of thermal expansion, pyroelectric and temperature change are shown by $\{\lambda\}$, $\{p\}$ and $\Delta\Theta$, respectively. Also, $\{C\}$, $\{e\}$ and $\{\in\}$ are the coefficients of elastic, piezoelectric and dielectric, respectively. Eq. (1) can be expanded in the following general form as

$$\begin{Bmatrix}\sigma_1\\ \sigma_2\\ \sigma_3\\ \tau_{23}\\ \tau_{31}\\ \tau_{12}\\ D_1\\ D_2\\ D_3\end{Bmatrix}=\begin{Bmatrix}C_{11} & C_{12} & C_{13} & 0 & 0 & 0 & 0 & 0 & -e_{31}\\ C_{12} & C_{22} & C_{23} & 0 & 0 & 0 & 0 & 0 & -e_{32}\\ C_{13} & C_{23} & C_{33} & 0 & 0 & 0 & 0 & 0 & -e_{33}\\ 0 & 0 & 0 & C_{44} & 0 & 0 & 0 & -e_{24} & 0\\ 0 & 0 & 0 & 0 & C_{55} & 0 & -e_{15} & 0 & 0\\ 0 & 0 & 0 & 0 & 0 & C_{66} & 0 & 0 & 0\\ 0 & 0 & 0 & 0 & e_{15} & 0 & \in_{11} & 0 & 0\\ 0 & 0 & 0 & e_{24} & 0 & 0 & 0 & \in_{22} & 0\\ e_{31} & e_{32} & e_{33} & 0 & 0 & 0 & 0 & 0 & \in_{33}\end{Bmatrix}\times\begin{Bmatrix}\varepsilon_1\\ \varepsilon_2\\ \varepsilon_3\\ \gamma_{23}\\ \gamma_{31}\\ \gamma_{12}\\ E_1\\ E_2\\ E_3\end{Bmatrix}-\begin{Bmatrix}\lambda_1\\ \lambda_2\\ \lambda_3\\ \lambda_4\\ \lambda_5\\ \lambda_6\\ p_1\\ p_2\\ p_3\end{Bmatrix}\Delta\Theta \tag{2}$$

where the component of the electric field can be written in terms of scalar functions of electric potential ϕ as Ding and Chen (2001)

$$E=-\nabla\phi \tag{3}$$

in which ∇ is the gradient operator.

2.2 Nonlocal elasticity theory

Small scale effects are studied in micro and nano mechanic usually by Eringen's nonlocal theory (Eringen 1983). Based on nonlocal elasticity theory, the stress tensor at a reference point of a body depends on the strain component at all of the points of the body. The relation between classical and nonlocal stresses is presented as follows

$$\begin{aligned}(1-(e_0a)^2\nabla^2)\sigma_{Nonlocl}&=\sigma_{Classical}\\(1-(e_0a)^2\nabla^2)D_{Nonlocl}&=D_{Classical}\end{aligned} \tag{4}$$

where ∇^2 is the Laplace operator and e_0a is known as small scale parameter which is specially depends on the internal characteristic length "a" of the micro/nanotube (e.g., distance between carbon-carbon bonds, granular size, lattice parameter). The right-hand side of Eq. (4) denotes the classical stress and electric displacement tensors which are obtained from Eq. (2). Because of the implicit nature of the Eq. (4) in this study we utilized an iterative-based method to obtain nonlocal stresses as follows

$$\begin{aligned}\sigma^{i+1}_{Nonlocal}&=(e_0a)^2\nabla^2\sigma^{i}_{Classical}+\sigma_{Classical}\\D^{i+1}_{Nonlocal}&=(e_0a)^2\nabla^2D^{i}_{Classical}+D_{Classical}\\\sigma^{0}_{Nonlocal}&=\sigma_{Classical}\\D^{0}_{Nonlocal}&=D_{Classical}\end{aligned} \tag{5}$$

where the iteration number *i* can start from zero, which is referred to the local stresses. Clearly, increasing the iteration number will be improved the accuracy of the nonlocal results. In addition, from now on we will use nonlocal components of stresses and electric displacement without using subscript.

2.3 Kinematic relations

Consider a circular cylindrical shell with length *L*, radius *R* and simply supported condition at both ends. According to nonlinear shallow shell models, the longitudinal ($\widetilde{U}$), circumfrential ($\tilde{V}$) and transverse ($\widetilde{W}$) displacement components of an arbitrary point of the shell are expressed as

$$\begin{aligned}\widetilde{U}(x,\theta,z,t)&=u(x,\theta,t)-z\frac{\partial w(x,\theta,t)}{\partial x}\\\tilde{V}(x,\theta,z,t)&=v(x,\theta,t)-z\frac{1}{R}\frac{\partial w(x,\theta,t)}{\partial \theta}\\\widetilde{W}(x,\theta,z,t)&=w(x,\theta,t)\end{aligned} \tag{6}$$

where u, v and w are the mid-plane displacements along x, θ and z coordinates, respectively and t is the time. Based on Donnell's nonlinear shell theory, the strain-displacement relations yield

$$\begin{cases}\varepsilon_x=\dfrac{\partial u}{\partial x}+\dfrac{1}{2}\left(\dfrac{\partial w}{\partial x}\right)^2+z\left(-\dfrac{\partial^2 w}{\partial x^2}\right)\\[2ex]\varepsilon_\theta=\dfrac{1}{R}\dfrac{\partial v}{\partial \theta}+\dfrac{w}{R}+\dfrac{1}{2R^2}\left(\dfrac{\partial w}{\partial \theta}\right)^2+z\left(-\dfrac{1}{R^2}\dfrac{\partial^2 w}{\partial \theta^2}\right)\\[2ex]\gamma_{x\theta}=\dfrac{1}{R}\dfrac{\partial u}{\partial \theta}+\dfrac{\partial v}{\partial x}+\dfrac{1}{R}\dfrac{\partial w}{\partial \theta}\dfrac{\partial w}{\partial x}+z\left(-\dfrac{2}{R}\dfrac{\partial^2 w}{\partial x\partial \theta}\right)\end{cases} \tag{7}$$

2.4 Mode expansion of displacements and electric potential

Considering simply supported boundary conditions at both ends of the cylindrical shell, the following mode expansion for components of displacement may be considered (Kurylov and Amabili 2010)

$$\begin{aligned}u&=\sum_{m=1}^{M}\sum_{n=0}^{N}sin\left(\frac{(2m-1)\pi x}{L}\right)[U^c_{mn}(t)\,cos(n\theta)+U^s_{mn}(t)\,sin(n\theta)]\\v&=\sum_{m=1}^{M}\sum_{n=0}^{N}sin\left(\frac{(2m-1)\pi x}{L}\right)[V^c_{mn}(t)\,cos(n\theta)+V^s_{mn}(t)\,sin(n\theta)]\\w&=\sum_{m=1}^{M}\sum_{n=0}^{N}sin\left(\frac{(2m-1)\pi x}{L}\right)[W^c_{mn}(t)\,cos(n\theta)+W^s_{mn}(t)\,sin(n\theta)]\end{aligned} \tag{8}$$

where m and n denote the longitudinal half wave number and circumferential wave number, respectively, and M and N are the maximum values of wave numbers. $U^c_{mn}(t)$, $U^s_{mn}(t)$, $V^c_{mn}(t)$, $V^s_{mn}(t)$, $W^c_{mn}(t)$ and $W^s_{mn}(t)$ are the time-dependent degrees of freedom (DOF) and $\{q_d\} = [U^c_{mn}(t), U^s_{mn}(t), V^c_{mn}(t), V^s_{mn}(t), W^c_{mn}(t), W^s_{mn}(t)]$ is defined as the vector of DOF. The vector dimension of $\{q_d\}$ denotes number of DOF which may be calculated as $N^{DOF} = 3\times(2M\times N+M)$. For electric potential ϕ the following mode expansion can be proposed (Alinia and Ghannadpour 2009)

$$\phi=\phi_0\left(1-\frac{x}{L}\right)+\sum_{m=1}^{M}\phi^s_m\,sin\left(\frac{(2m-1)\pi x}{L}\right) \tag{9}$$

where ϕ^s_m is the time-independent amplitude component of electric potential and $\{q_\phi\}=\{\phi^s_m\}$ is defined as the vector of electric potential amplitudes and ϕ_0 indicates the magnitude of imposed electric potential. Because of the unidirectional longitudinally polarized electric field, the electric potential is expanded as a function of the longitudinal coordinate *x*. In the numerical results section, the accuracy of the results will be examined for different values of *M* and *N*.

In addition, a vector of unknowns can be introduced as follows

$$\{q\}=\left\{\{q_d\},\{q_\phi\}\right\}^T \tag{10}$$

2.5 Energy functions

Based on the theory of piezoelectricity the total potential and kinetic energies of the micro shell with length *L*, cross section *A*, volume $\forall$ and density ρ_s are obtained as Yang

(2005)

$$U_S = \frac{1}{2}\int_0^L \int_A [\sigma D]\begin{Bmatrix}\varepsilon \\ -E\end{Bmatrix} dAdx \quad (11)$$

$$T_S = \frac{1}{2}\rho_S \iiint_{\forall} \vec{V}.\vec{V}\, d\forall \quad (12)$$

where σ and D are nonlocal components of stress and electric displacement and obtained from Eq. (5). In addition, $\vec{V}$ corresponds the velocity vector of the micro shell which leads to the following relation.

$$T_S = \frac{1}{2}\rho_S \int_0^L \int_A \left[\left(\frac{\partial u}{\partial t} - z(\frac{\partial^2 w}{\partial x \partial t})\right)^2 + \left(\frac{\partial w}{\partial t}\right)^2\right] dAdx \quad (13)$$

The external works done by the surrounded elastic foundation are expressed as

$$W_{elastic\ foundation} = \frac{1}{2}\int_0^L (-K_W w + G_P \nabla^2 w) w dx \quad (14)$$

where K_w and G_p are respectively, the Winkler's spring foundation modulus and Pasternak's shear foundation modulus. Moreover, the energies related with the fluid flow are evaluated separately in the following section.

3. Pulsating fluid flow modelling

In this study we consider a visco-pulsating micro fluid flow inside the microshell which is one of the most empirical models. The micro fluid flow is assumed to be turbulent, fully developed, Newtonian, irrotational, isentropic and incompressible. The unsteady fluid motion is obtained based on potential flow theory and for more reality of the micro scale problem the effects of pulsating viscosity and slip boundary condition are applied based on unsteady time-averaged Navies-Stokes equations and Knudsen number theory (Amabili 2008, Gu *et al*. 2016).

Let us assume no cavitation occurred at the fluid and shell interfaces. An unsteady potential function φ may be found which is satisfied the Laplace equation and following boundary condition (Fox *et al*. 2008) as

$$\nabla^2\varphi = \frac{\partial^2\varphi}{\partial x^2} + \frac{\partial^2\varphi}{\partial r^2} + \frac{1}{r}\frac{\partial\varphi}{\partial r} + \frac{1}{r^2}\frac{\partial^2\varphi}{\partial\theta^2} = 0 \quad (15)$$

$$\frac{\partial\varphi}{\partial r}\Big|_{r=R} = \left(\frac{\partial w}{\partial t} + U_f\frac{\partial w}{\partial x}\right) \quad (16)$$

where U_f is the pulsating flow velocity. Employing the separation of variables method the general solution of Eq. (14) may be obtained as

$$\varphi(x,r,\theta,t) = \sum_{m=1}^{M}\sum_{n=0}^{N} \Phi_m(x)\Xi_{m,n}(r)\cos(n\theta)\, f_{m,n}(t) \quad (17)$$

Substituting Eq. (17) into Eq. (15) beside applying the regularity condition at $r = 0$, the unknown functions will be obtained. Utilizing the boundary condition Eq. (16), Eq. (17) will be evaluated as

$$\varphi(x,r,\theta,t) = \sum_{m=1}^{M}\sum_{n=0}^{N} \frac{L}{m\pi}\frac{I_n(m\pi r/L)}{I'_n(m\pi R/L)}\left(\frac{\partial w_{m,n}}{\partial t} + U_f\frac{\partial w_{m,n}}{\partial x}\right) \quad (18)$$

where I_n and I'_n are respectively the modified Bessel function of the first kind of order n and its derivative. Consequently, the perturbation pressure at the inner wall of shell is found as Amabili (2008)

$$p = -\rho_F \sum_{m=1}^{M}\sum_{n=0}^{N} \frac{L}{m\pi}\frac{I_n(m\pi r/L)}{I'_n(m\pi R/L)}\left(\frac{\partial}{\partial t} + U_f\frac{\partial}{\partial x}\right)^2 w_{m,n} \quad (19)$$

in which ρ_F is the density of fluid flow.

3.1 Potential energy of fluid flow

Consider the fluid flow inside the micro shell with occupied volume Γ and surrounded surface Λ. The total energy related to the fluid-flow E_F^T is given by

$$E_F^T = \frac{1}{2}\rho_f \iiint_{\Gamma} \vec{V}_f.\vec{V}_f\, d\Gamma \quad (20)$$

According to the Green's theorem, Eq. (20) is evaluated as

$$E_F^T = \frac{1}{2}\rho_f \iiint_{\Gamma} \nabla\Psi.\nabla\Psi\, d\Gamma = \frac{1}{2}\rho_f \iint_{\Lambda}\left(\Psi\frac{\partial\Psi}{\partial\upsilon}\right) d\Lambda \quad (21)$$

where Ψ is the potential function of the fluid flow and υ is the normal vector of boundary surfaces which is considered positive outward. Integrating of Eq. (21) gives

$$\begin{aligned} E_F^T = {} & \frac{1}{2}\rho_f \int_0^{2\pi}\int_0^L \left(\Psi\frac{\partial\Psi}{\partial r}\right)_{r=R} dx\, Rd\theta \\ & + \frac{1}{2}\rho_f \int_0^{2\pi}\int_0^R \left(\Psi\frac{\partial\Psi}{\partial x}\right)_{x=L} r dr\, d\theta \\ & - \frac{1}{2}\rho_f \int_0^{2\pi}\int_0^R \left(\Psi\frac{\partial\Psi}{\partial x}\right)_{x=0} r dr\, d\theta \end{aligned} \quad (22)$$

in which the boundary conditions are

$$\begin{aligned} & \frac{\partial\Psi}{\partial r} = \frac{\partial\varphi}{\partial r}, \qquad \frac{\partial\Psi}{\partial x} = U_f + \frac{\partial\varphi}{\partial x} \\ & \Psi\left|U_f L + \varphi\right|_{x=L} \\ & \Psi|\varphi|_{x=L} \end{aligned} \quad (23)$$

Using Eq. (23), Eq. (22) may be obtained as

$$E_F^T = E_F^p + \frac{1}{2}\rho_f \int_0^{2\pi}\int_0^L \left(U_f x\frac{\partial\varphi}{\partial r}\right)_{r=R} dx\, Rd\theta \quad (24)$$

$$+\frac{1}{2}\rho_f\int_0^{2\pi}\int_0^{R}\left(U_f L\frac{\partial\varphi}{\partial x}\right)_{x=L} r dr\, d\theta$$
$$+\frac{1}{2}\rho_f U_f^2\pi R^2 L$$

where E_F^p denotes the perturbation velocity potential of fluid and is given by

$$E_F^p=\frac{1}{2}\rho_f\int_0^{2\pi}\int_0^{L}\left(\varphi\frac{\partial\varphi}{\partial r}\right)_{r=R} dx\, R d\theta \tag{25}$$

Moreover, other terms in Eq. (24) have no influence to the total energy of fluid flow. Substituting Eq. (15) into Eq. (16) and employing Eq. (6) yields

$$E_F^p=\frac{1}{2}\rho_f\int_0^{2\pi}\int_0^{L}(\varphi)_{r=R}\left(\frac{\partial w}{\partial t}+U_f\frac{\partial w}{\partial x}\right)dx\, R d\theta \tag{26}$$

Using Eq. (8), Eq. (26) may be obtained as

$$E_F^p=\frac{1}{2}\rho_f\int_0^{2\pi}\int_0^{L}\sum_{m=1}^{M}\sum_{l=1}^{M}\sum_{n=0}^{N}\sum_{k=0}^{N}\frac{L}{m\pi}\frac{I_n(m\pi R/L)}{I'_n(m\pi R/L)} \times\left(\dot{w}_{m,n}+U_f\frac{\partial w_{m,n}}{\partial x}\right)\left(\dot{w}_{l,k}+U_f\frac{\partial w_{l,k}}{\partial x}\right)dxRd\theta \tag{27}$$

Substituting Eq. (27) in Eq. (24) the total energy of fluid is derived and divided as

$$E_F^T=T_F-V_F+E_G \tag{28}$$

where T_F, E_G and V_F are kinetic, gyroscopic and potential energies of the fluid flow, respectively and are expressed as follows

$$T_F=\frac{1}{2}\rho_f\sum_{m=1}^{M}\sum_{n=0}^{N}\int_0^{2\pi}\int_0^{L}\frac{L}{m\pi}\frac{I_n(m\pi R/L)}{I'_n(m\pi R/L)}\dot{w}_{m,n}^2\, dxRd\theta \tag{29}$$

$$V_F=-\frac{1}{2}\rho_f\sum_{m=1}^{M}\sum_{n=0}^{N}\int_0^{2\pi}\int_0^{L}\frac{L}{m\pi}\frac{I_n(m\pi R/L)}{I'_n(m\pi R/L)}U_f^2\left(\frac{\partial w_{m,n}}{\partial x}\right)^2 dxRd\theta \tag{30}$$

$$E_G=\frac{1}{2}\rho_f\sum_{m=1}^{M}\sum_{l=1}^{M}\sum_{n=0}^{N}\sum_{k=0}^{N}\int_0^{2\pi}\int_0^{L}\frac{L}{m\pi}\frac{I_n\left(\frac{m\pi R}{L}\right)}{I'_n\left(\frac{m\pi R}{L}\right)} \times U_f\left(\dot{w}_{m,n}\frac{\partial w_{l,k}}{\partial x}+\dot{w}_{l,k}\frac{\partial w_{m,n}}{\partial x}\right)dxRd\theta \tag{31}$$

The unsteady flow velocity $U_f(t)$ for pulsating fluid flow is expressed by the following time dependent function as

$$U_f(t)=U_0(1+\xi\cos(\Omega t)) \tag{32}$$

where U_0 is the mean value of flow velocity, ξ is the amplitude of the harmonic fluctuation and Ω is its frequency. In addition, it is clear that the expressions of T_F, E_G and V_F will be time dependent in this case and therefore, this leads to the addition of a new term in the Lagrange equations of motion in section 4.

3.2 Viscous effects for pulsitule flow

In this section, the pulsating fluid viscosity effect is simulated as an external force acts on the inner wall of the shell. Considering a fully developed turbulent and incompressible axial flow regime with fluctuating velocities $\bar{u}_x, \bar{u}_\theta, \bar{u}_r$ respectively in the axial, circumferential and radial directions, the time-averaged Navier-Stokes equations are given by

$$\frac{1}{\rho_f}\frac{\partial P}{\partial x}=-\frac{1}{r}\frac{d}{dr}(r\bar{u}_x\bar{u}_r)+\frac{\eta}{r}\frac{d}{dr}\left(r\frac{dU_f}{dr}\right)$$
$$\frac{1}{\rho_f}\frac{\partial P}{\partial r}=-\frac{1}{r}\frac{d}{dr}\left(r\bar{u}_r{}^2\right)+\frac{\bar{u}_\theta^2}{r} \tag{33}$$
$$0=\frac{d}{dr}(r\bar{u}_r\bar{u}_\theta)+2\frac{\bar{u}_r\bar{u}_\theta}{r}$$

where η is kinematic viscosity and the overbar indicates the time-averaged components. In the following, by using the Computational Fluid Dynamics (CFD) the Pressure distribution will be obtained as Paidoussis *et al.* (1985)

$$P(x,r)=-2\frac{\rho_f}{R}U_\tau^2 x-\rho_f\bar{u}_r^2+\rho_f\int_R^r\frac{\bar{u}_\theta{}^2-\bar{u}_r{}^2}{r}dr+P(0,R) \tag{34}$$

where the stress velocity U_τ is expressed as

$$U_\tau=\left(-\eta\frac{dU_f}{dr}\right)_{r=R}^{1/2}=\left(\frac{\tau_w}{\rho_f}\right)^{1/2}=\left(\frac{1}{8}fU_f^2\right)^{1/2} \tag{35}$$

in which f and τ_w are respectively, the friction factor and the fluid frictional force per unit area of the shell. The distribution of pressure on the shell interfaces as well as the drop pressure in the axial direction of the shell are given by

$$P(x,R)=-2\frac{\rho_f}{R}U_\tau^2 x+P(0,R)=-\rho_f\left(\frac{f}{4R}U_f^2+\frac{dU_f}{dt}\right)x+P(0,R) \tag{36}$$

$$\Delta P_w=P(0,R)-P(L,R)=\rho_f\left(\frac{f}{4R}U_f{}^2+\frac{dU_f}{dt}\right)L \tag{37}$$

Ignoring the effects of flow acceleration, the friction shear stress in the axial direction is given by

$$\tau_w=f\rho_f\frac{U_f{}^2}{8} \tag{38}$$

Based on classical fluid mechanic the friction factor (f) of the micro shell is function of the Reynolds number (Re) and the mean roughness (δ) of the inner wall of the shell. Using empirical Colebrook equation, the friction factor is

estimated by

$$\frac{1}{\sqrt{f}} + 2\,log\left(\frac{\delta/2R}{3.7} + \frac{2.51}{Re\sqrt{f}}\right) = 0 \tag{39}$$

in which $Re = 2RU_f/\eta$.

Lastly the total work associated with the fluid viscosity is given by

$$W_{\text{Fluid Viscosity}} = \int_0^{2\pi}\int_0^{L} (\Delta P_W + \tau_W u)\, dxRd\theta \tag{40}$$

3.3 Effect of slip boundary conditions

Often the FSI problems are assumed with no-slip boundary conditions in the fluid and shell interfaces. However, this assumption will not be valid for the micro scale problems due to the nonlocality and Knudsen number effects (Karniadakis *et al*. 2005). In other words, based on Kn theory the value of Kn in micro scale problems will be exceed from 0.01 and therefore an average fluid Velocity Correction Factor (VCF) should be applied in all of the following equations as Rashidi (2012)

$$VCF = \frac{V_{avg,slip}}{V_{avg,no-slip}} = \left(4\left(\frac{2-\sigma_v}{\sigma_v}\right)\left(\frac{Kn}{1+Kn}\right)+1\right) \tag{41}$$

where σ_v is the tangential momentum accommodation coefficient and for most practical purposes is measured to be 0.7 (Shokouhmand *et al*. 2010).

4. Solution procedure

The modified Lagrange equations of motion for open systems conveying fluid is given by

$$\begin{aligned}&\frac{d}{dt}\left[\frac{\partial(T_S+T_F+E_G)}{\partial \dot{q}_k}\right] - \frac{\partial(T_S+T_F+E_G)}{\partial q_k}\\ &+\frac{\partial(U_S+V_F)}{\partial q_k} = Q_k, k = 1,\ldots,3N\end{aligned} \tag{42}$$

in which q_k is the elements of vector $\{q\}$ that is introduced in section 2.5, the terms $\partial T_S/\partial q_k$ and $\partial T_F/\partial q_k$ are zero and Q_k is the generalized forces obtained by differentiation of the virtual work W done by external forces

$$Q_k = \frac{\partial W}{\partial q_k} \tag{43}$$

Employing mode expansions Eqs. (8) and (9), Eq. (42) is evaluated as follows

$$[M]\{\ddot{q}\} + [C(t)]\{\dot{q}\} + [K(t)]\{q\} = \{Q\} \tag{44}$$

where $[M]$ and $[C(t)]$ are respectively the mass and $[K(t)]$ damping matrices and is the stiffness matrix composed of linear and nonlinear terms as

$$[K(t)] = [K_L(t) + K_{NL}(t)] \tag{45}$$

According to lack of external electrical load the second set of Eq. (46) leads

$$\begin{aligned}&\begin{bmatrix}M_{dd} & 0\\ 0 & 0\end{bmatrix}\begin{Bmatrix}\ddot{q}_d\\ \ddot{q}_\phi\end{Bmatrix} + \begin{bmatrix}C_{dd} & 0\\ 0 & 0\end{bmatrix}\begin{Bmatrix}\dot{q}_d\\ \dot{q}_\phi\end{Bmatrix}\\ &+\begin{bmatrix}K_{dd} & K_{d\phi}\\ K_{\phi d} & K_{\phi\phi}\end{bmatrix}\begin{Bmatrix}q_d\\ q_\phi\end{Bmatrix} = \begin{Bmatrix}Q_d\\ Q_\phi\end{Bmatrix}\end{aligned} \tag{46}$$

According to lack of external electrical load the second set of Eq. (46) leads

$$\{q_\phi\} = -\left[K_{\phi\phi}^{-1}K_{\phi d}\right]\{q_d\} \tag{47}$$

Utilizing Eq. (47), q_φ in the first sets of equations of Eq. (46) is eliminated and yields a set of modified equations of motion as

$$[M_{dd}]\{\ddot{q}_d\} + [C_{dd}(t)]\{\dot{q}_d\} + [K_M(t)]\{q_d\} = \{Q_M\} \tag{48}$$

where

$$\begin{aligned}K_M &= K_{dd} - K_{d\varphi}K_{\varphi\varphi}^{-1}K_{\varphi d}\\ Q_M &= Q_d - K_{d\phi}K_{\phi\phi}^{-1}Q_\phi\end{aligned} \tag{49}$$

It is to be mentioned that, the nonlinear modified stiffness matrix $[K_M(t)]$ and the damping matrix $[C_{dd}(t)]$ in Eq. (48) are harmonically time dependent by considering the pulsatile flow regime according to Eq. (33) as

$$\begin{aligned}K_M(t) &= f_1(sin\,\Omega\, t, cos\,\Omega\, t),\\ C_{dd}(t) &= f_2(sin\,\Omega\, t, cos\,\Omega\, t)\end{aligned} \tag{50}$$

4.1 Electro-thermo-dynamical response analyses

The N^{DOF} nonlinear second-order ordinary differential Eq. (48) can be simplified to $2\times N^{DOF}$ nonlinear first-order ordinary differential equations by introducing dummy variable y_k as follows

$$\begin{cases}\dot{q}_k = y_k\\ \dot{y}_k = -M_{k,m}^{-1}C_{dd_{m,j}}q_j - M_{k,m}^{-1}K_{M_{m,j}}q_j + M_{k,m}^{-1}Q_{Mm}\end{cases} \tag{51}$$

Integrating Eq. (51) via the fourth order Runge-Kutta method and with a step size 0.0001 leads to the nonlinear electro-thermo-dynamical response of the system. The initial conditions of displacement are considered by distributing the parabolic function with the maximum displacement value in the similar equivalent beam.

4.2 Dynamic instability formulation

For static fluid velocity condition ($\xi = 0$), the following general solution can be expressed for Eq. (48) as

$$\{q_d\} = \{\hat{q}_d\}exp(\omega t) \tag{52}$$

in which $\{\hat{q}_d\}$ is the amplitudes of the displacements vector and ω is complex circular frequency composed of real and imaginary parts representing damping and natural frequencies, respectively.

Introducing the secondary vector $\{S\} = \omega\{q_d\}$, Eq. (48) is converted to the following state space problem as

$$[\Psi]\{X\} = \omega\{X\} \tag{53}$$

where

$$[\Psi] = \begin{bmatrix} 0I \\ -M_{dd}^{-1}K_M - M_{dd}^{-1}C_{dd} \end{bmatrix} \qquad \{X\} = [\{q_d\}, \{S\}]^T \tag{54}$$

Eq. (53) is an eigenvalue problem with nonlinear stiffness terms that can be solved according to the following iterative procedure (Yang *et al*. 2010).

Step 1: Calculating linear eigenvalues and eigenvectors by ignoring all of the nonlinear terms in the stiffness matrix.

Step 2: Scaling up the eigenvectors and estimating nonlinear terms in the stiffness matrix.

Step 3: Considering nonlinear and linear components of the stiffness matrix together and evaluating eigenvectors and eigenvalues of the updated eigenvalue problem.

Step 4: Comparing new and previous eigenvectors until reaching the convergence conditions and in otherwise step 2 to 4 must be repeated.

In this study, above procedure is done until the maximum relative error between two successive iterations becomes less than 0.1%.

4.3 Parametric instability formulation

In order to study the parametric instability of the system it is usual to study the effects of amplitude (ξ) and frequency (Ω) of the pulsating flow on the system stability at various static fluid velocity levels. The boundaries of the regions of parametric resonance may be obtained usually via the Bolotin (1964) or Floquet methods. Based on Bolotin's method, the generalized coordinate is assumed to be periodic and is expressed in the following form

$$q_d(t) = \sum_{k=0}^{\bar{N}} \left\{ a_k \, sin\left(\frac{k\Omega t}{2}\right) + b_k \, cos\left(\frac{k\Omega t}{2}\right) \right\} \tag{55}$$

Substituting Eq. (55) into Eq. (48) and setting the coefficients of harmonics to zero, the following algebraic equation is obtained

$$[C]\{Y\} = \{0\} \tag{56}$$

where $\{Y\} = \{b_0, a_1, b_1, \ldots, a_{\bar{N}}, b_{\bar{N}}\}^T$ is the amplitude vector. The characteristic equation of this problem is expressed as

$$f(C) = det(C) = 0 \tag{57}$$

This equation is a nonlinear algebraic equation on Ω, which is solved numerically by the mathematical software to detect the system's parametric resonance instability boundaries.

Table 1 Properties of PZT4

Properties of PZT4	Shokouhmand *et al.* (2010)
C_{11}(GPa)	139
C_{22}(GPa)	115
C_{12}(GPa)	77.8
e_{11}(C/m^2)	15.1
e_{12}(C/m^2)	-5.2
$\in_{11}$ (C^2/Nm^2)	6.46×10^{-9}
$p_{11}(C/m^2K)$	-2.5×10^{-5}
α_1(1/K)	7.41×10^{-6}
α_2(1/K)	2.11×10^{-6}
ρ(Kg/m^3)	7500
L/R	20

5. Numerical results

The dynamical instabilities and electro-dynamical response of a smart micro shell surrounded by an elastic foundation and under internal pulsating micro flow (i.e., sinusoidal function) as well as axial electric field (as shown in Fig. 1) are examined in this section. To this end, divergence and flutter instabilities which are occurred by increasing the mean flow velocity (U_0) as well as parametric resonance instability in the case of increasing dimensionless pulsation amplitude (ξ) are studied. The micro shell is considered to be made of piezoelectric materials e.g., PZT4 and its structural properties are given in Table 1. A comprehensive parametric study has been made focusing on the combined effects of small-scale parameter, elastic foundation modules, Knudsen number, fluid viscosity, geometric nonlinearity and applied electric field. In Table 2 the accuracy of the results is examined for different magnitudes of M and N and for both linear and nonlinear approaches. From this table, it can be concluded that the accuracy of the results is sufficiently enough for linear analyses if $(M, N) = (1,1)$ (i.e., DOF = 9) and for nonlinear analyses if $(M, N) = (3,1)$ (i.e., DOF = 27). Now, let us to introduce the dimensionless parameters used in this study as follows

$$\begin{gathered} U_0^* = U_0\sqrt{\frac{\rho_f}{C_{11}}}, \qquad \Omega^* = \Omega L\sqrt{\frac{\rho}{C_{11}}} \\ \omega^* = \omega L\sqrt{\frac{\rho}{C_{11}}}, \qquad \eta = \frac{e_0 a}{L} \\ \mu^* = \frac{\mu A_f}{\sqrt{EIm_f}}, \qquad K_w^* = \frac{K_w}{C_{11}} \\ G_P^* = \frac{G_P}{C_{11}Rh} \\ \bar{W} = \frac{w}{L} \qquad\qquad \bar{X} = \frac{x}{L}, \end{gathered} \tag{58}$$

The results will be presented in the dimensionless form.

Table 2 Accuracy of the results for various number of mode expansion

M	$N(U_0^*=0.0001,\xi=0)$			$N(U_0^*=0.001,\xi=0)$		
	1	2	3	1	2	3
1	$N^{DOF}=9$ $Im(\omega^*)_{NL}=0.00934$ $Im(\omega^*)_L=0.00925$	$N^{DOF}=15$ $Im(\omega^*)_{NL}=0.00942$ $Im(\omega^*)_L=0.00925$	$N^{DOF}=21$ $Im(\omega^*)_{NL}=0.00947$ $Im(\omega^*)_L=0.00925$	$N^{DOF}=9$ $Im(\omega^*)_{NL}=0.00498$ $Im(\omega^*)_L=0.00460$	$N^{DOF}=15$ $Im(\omega^*)_{NL}=0.00523$ $Im(\omega^*)_L=0.00460$	$N^{DOF}=21$ $Im(\omega^*)_{NL}=0.00537$ $Im(\omega^*)_L=0.00460$
2	$N^{DOF}=18$ $Im(\omega^*)_{NL}=0.00943$ $Im(\omega^*)_L=0.00925$	$N^{DOF}=30$ $Im(\omega^*)_{NL}=0.00946$ $Im(\omega^*)_L=0.00925$	$N^{DOF}=42$ $Im(\omega^*)_{NL}=0.00950$ $Im(\omega^*)_L=0.00925$	$N^{DOF}=18$ $Im(\omega^*)_{NL}=0.00531$ $Im(\omega^*)_L=0.00460$	$N^{DOF}=30$ $Im(\omega^*)_{NL}=0.00542$ $Im(\omega^*)_L=0.00460$	$N^{DOF}=42$ $Im(\omega^*)_{NL}=0.00548$ $Im(\omega^*)_L=0.00460$
3	$N^{DOF}=27$ $Im(\omega^*)_{NL}=0.00950$ $Im(\omega^*)_L=0.00925$	$N^{DOF}=45$ $Im(\omega^*)_{NL}=0.00950$ $Im(\omega^*)_L=0.00925$	$N^{DOF}=63$ $Im(\omega^*)_{NL}=0.00950$ $Im(\omega^*)_L=0.00925$	$N^{DOF}=27$ $Im(\omega^*)_{NL}=0.00550$ $Im(\omega^*)_L=0.00460$	$N^{DOF}=45$ $Im(\omega^*)_{NL}=0.00552$ $Im(\omega^*)_L=0.00460$	$N^{DOF}=63$ $Im(\omega^*)_{NL}=0.00552$ $Im(\omega^*)_L=0.00460$

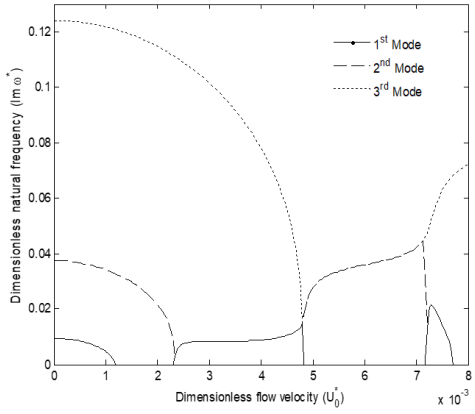

(a) Imaginary part of frequencies

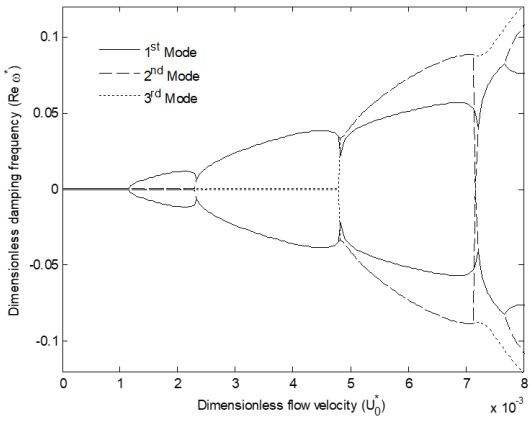

(b) Real part of frequencies

Fig. 2 Dimensionless frequencies versus dimensionless flow velocity for 1st to 3rd mode

5.1 Modal analyses and critical flow velocity for the case of static fluid case $(\xi=0)$

Effects of increasing U_0^* on the natural and damping frequencies of the smart micro shell for the first three vibrational modes are studied in Figs. 2(a) and (b). As can be seen from these figures, by increasing U_0^*, the imaginary part of natural frequencies will be decreased until reaching the value zero at $U_0^*=0.0012$, 0.0023 and 0.0048 (for the first, second and third mode, respectively) which are introduced the critical flow velocities. It is clear from Fig. 2(b) that, in these points the real part of frequencies becomes nonzero and divergence instability will be occurred. For more clarity, let us to consider the increasing flow velocity for the first mode (fundamental mode). In this mode and at first, the imaginary part of frequency will be decreased by increasing flow velocity which means less stable conditions. The critical flow velocity will be $U_0^*=0.0012$ and the divergence instability occurred via a pitchfork bifurcation point as shown in Fig. 2(b). In addition, by more increasing flow velocities we can see for the range of $0.0012<U_0^*<0.0048$ the first and second modes will be merged which is another kind of instabilities known as flutter instability. This matter will be occurred more in higher flow velocities.

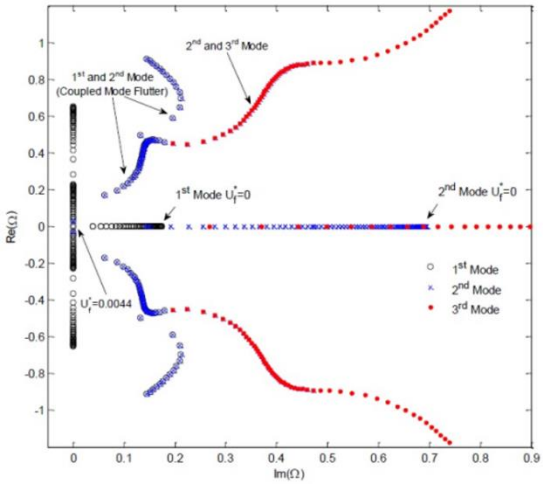

Fig. 3 Complex frequencies on Im-Re plane for the first 3 vibration modes

In Fig. 3, the stability of the system is also investigated on the Im-Re plane for the first three vibration modes when the flow velocity is increased incrementally from zero. It is clear to any dynamic system that with no-initial condition and in the absence of all other kind of external excitations (i.e., flow velocity is zero), the system should be stable. This fact is proved in this figure due to the imaginary nature of the complex frequency when the flow velocity is being increased from zero. In this case the complex frequencies are moved horizontally backward on the imaginary axes until reaching the value zero on the origin of the plane. In

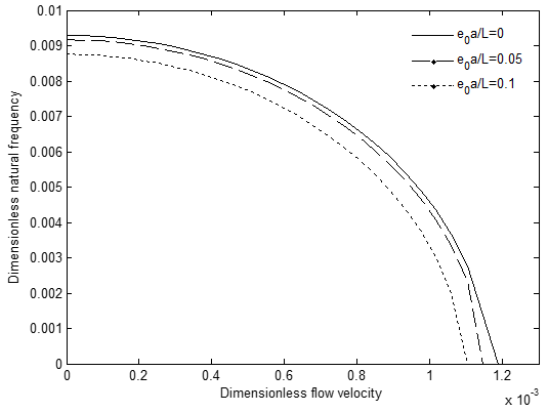

Fig. 4 Dimensionless flow velocity versus dimensionless natural frequency for various small-scale parameter for $\xi = 0$

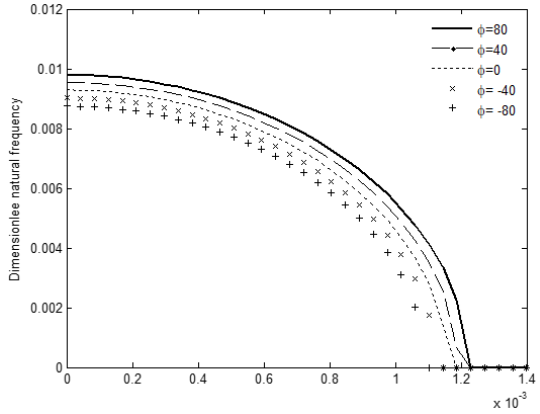

Fig. 6 Dimensionless flow velocity versus dimensionless natural frequency for various applied voltage for $\xi = 0$

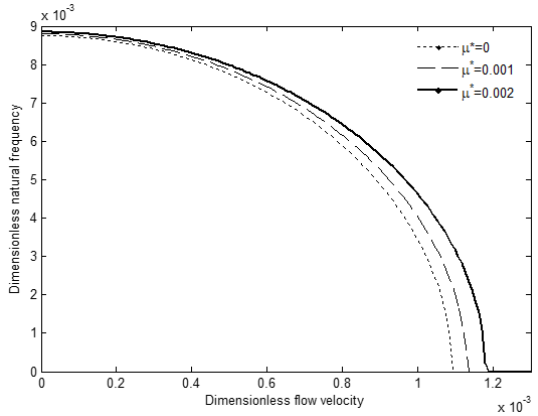

Fig. 5 Dimensionless flow velocity versus dimensionless natural frequency for various magnitudes of fluid viscosity for $\xi = 0$

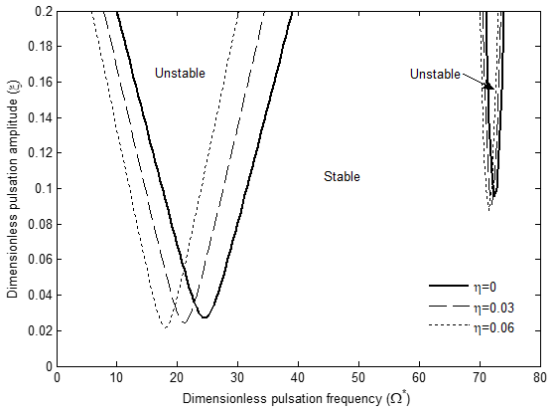

Fig. 7 Instability region of smart micro shell for $U_0^* = 0.0001$ (right side) and $U_0^* = 0.001$ (left side) and various dimensionless small-scale parameters

this point the real part of the complex frequency becomes non zero and the divergence instability will be observed clearly. Moreover, as the flow velocity increases again the complex frequencies moves vertically on the real axes and then return to the origin to restore the stability again. However as mentioned in Fig. 2, the flutter instability is occurred in this point by merging the results of first and second modes.

Fig. 4. depicts the effects of small-scale parameter on the fundamental frequency and the critical flow velocity. As can be seen by increasing flow velocity the frequency and the critical flow velocity will be decreased by an increasing rate.

The variation of the fluid viscosity magnitude is demonstrated in Fig. 5. It can be observed that the influence of viscosity becomes more remarkable when the fluid velocity is increased. Additionally, the fundamental frequency as well as the critical flow velocity of the system will be increased when the viscosity of fluid is increased which means that the stability of the system is improved. The Effects of external applied voltage on the fundamental frequency are shown in Fig. 6. It is concluded that at a constant flow velocity applying positive (direct) electric potential increase the fundamental frequency and also the critical flow velocity which means that the stability of the system is increased. It is also found that imposing negative (indirect) electric potential decrease the fundamental frequency of the system. This statement means that applying external electric field is an effective controlling parameter for the smart fluid conveying systems

5.2 Parametric instability of dynamic fluid case ($\xi \neq 0$)

By enhancing the dimensionless pulsation amplitude of fluid flow (ξ), the parametric resonance instability will be happened and its boundary curves are achieved from Eq. (57). It is more common from previous literatures that the results of these analyses will be examined in the frequency Ω amplitude ξ plane at various fixed level of all other influencing parameters such as mean flow velocity, viscosity, small scale parameter and etc. Figs. 7 to 11 show the instability boundary curves for the system. From all of this figures, the regions outside and inside the curves is related to stable and unstable conditions, respectively. As can be seen from these figures, by increasing the mean flow

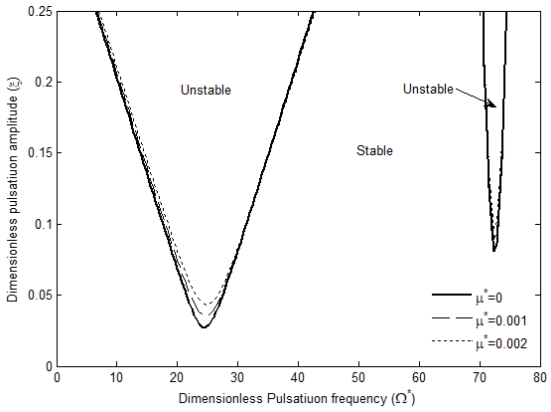

Fig. 8 Instability boundaries of smart micro shell for $U_0^* = 0.0001$ (right side) and $U_0^* = 0.001$ (left side) and various dimensionless fluid viscosities

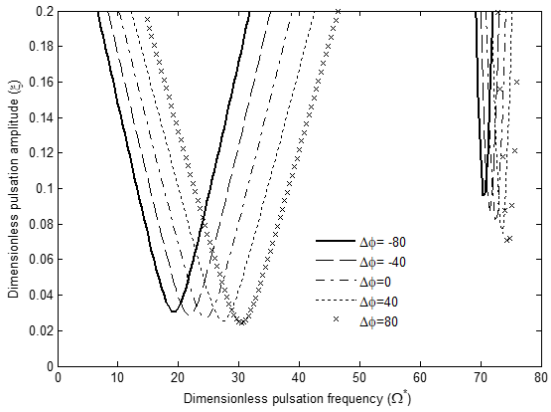

Fig. 9 Effects of applied electric field on instability boundaries of smart micro shell for $U_0^* = 0.0001$ (right side) and $U_0^* = 0.001$ (left side)

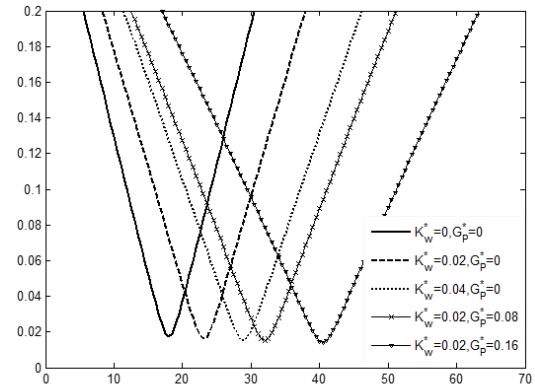

Fig. 10 Effects of elastic medium on instability boundaries of smart micro shell for $U_0^* = 0.001$

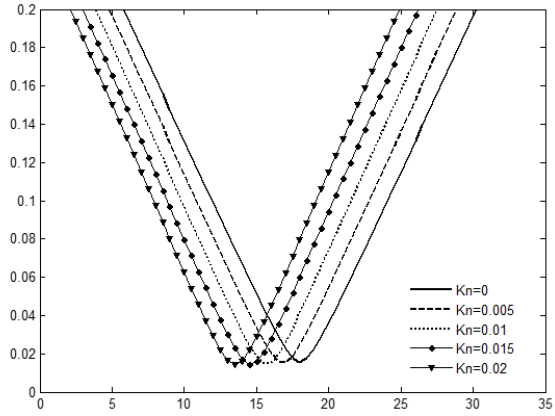

Fig. 11 Effects of Kn on instability boundaries of smart micro shell for $U_0^* = 0.001$

velocity the instability boundaries are moved to down and left and will be broaden than previous. This means that smaller pulsating amplitude as well as a wider range of pulsating frequencies leads to the instability.

Effects of small-scale parameter are specially studied in Fig 7. As can be seen from this figure, effects of nonlocality are more significant at higher flow velocities. It is shown that considering nonlocality affects the resonance regions move from higher frequencies to lower ones (toward left and slightly down). This means that the natural frequencies of the system are decreased. In addition, at a constant (ξ) the resonance region will be narrower than previous which means also more stable condition at this case.

Fig. 8 shows the instability boundaries of the viscous-fluid conveying beam. It is observed that the effects of fluid viscosity are strongly dependent to the mean flow velocity. As the mean flow velocity increased, influences of the fluid viscosity become more considerable. Additionally with increasing fluid viscosity, the area of instability region is decreased and instability boundaries are slightly shift right. It is occurred because of increasing natural frequencies of the system as was observed in Fig. 5.

To evaluate the effects of the piezoelectricity properties of the smart shell, the instability response of the system is obtained by applying direct and indirect external voltage. Fig. 9 illustrates the instability boundaries of the system under different applying voltages. It is found that by applying direct voltage the instability curves move right that means the resonance frequencies of the system are increased. In other words, direct voltage increases the stability of the system and indirect voltage vice versa.

Fig. 10 illustrate effects of both Winkler and Pasternak elastic foundations on instability boundaries of the system for $U_0^* = 0.001$. It is shown that the instability areas of the system shift to the left when the elastic foundation is existed. This fact is because of the stiffness of the elastic foundation absorbs the vibrating energy of the system and make a stiffer and more stable structure. Fig. 7 also depicts more stable condition from Pasternak foundation (which is considered both normal and shear effects) than Winkler foundation with only normal loads from.

For a micro fluid flow the value of Kn is in range of $10^{-2} < Kn < 10^{-1}$ and therefore the slippery regime will be occurred. It can be seen from Fig. 11, enhancing the value of Kn moves the instability area to the right and down which means lesser stability condition. In fact, increasing Kn means increasing the mean free path of fluid and results lower stiffness of the system.

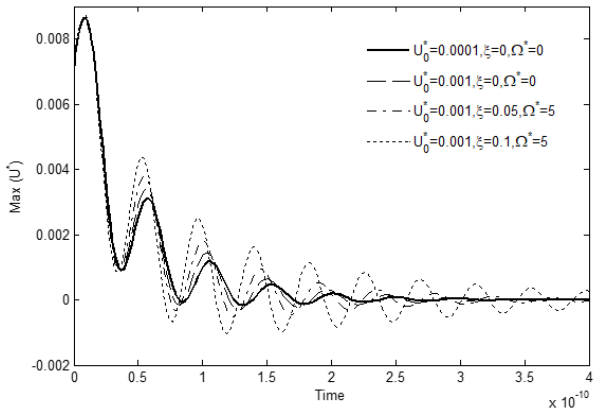

(a) Stable condition $U_0^* < U_{fc}$

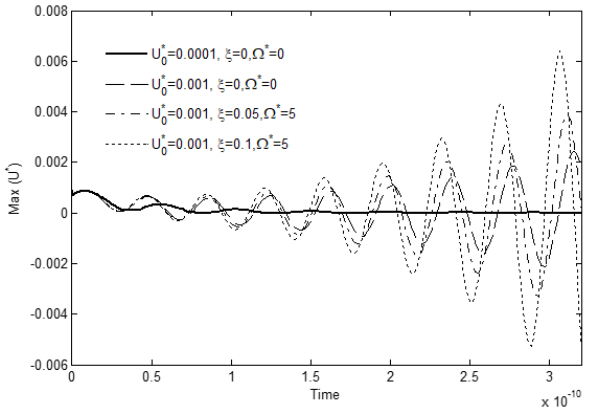

(b) Unstable condition $U_0^* > U_{fc}$

Fig. 12 Maximum amplitude of axial displacement for various fluid flow velocities

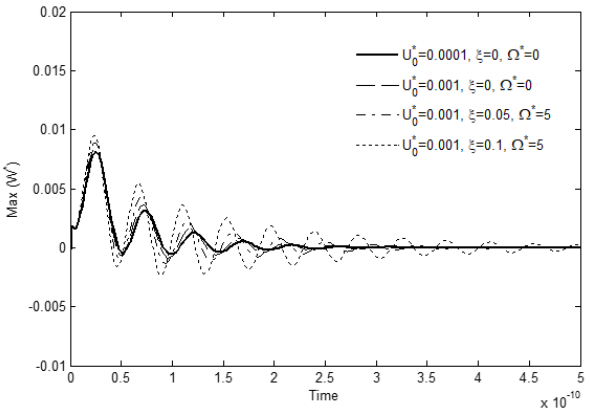

(a) Stable condition $U_0^* < U_{fc}$

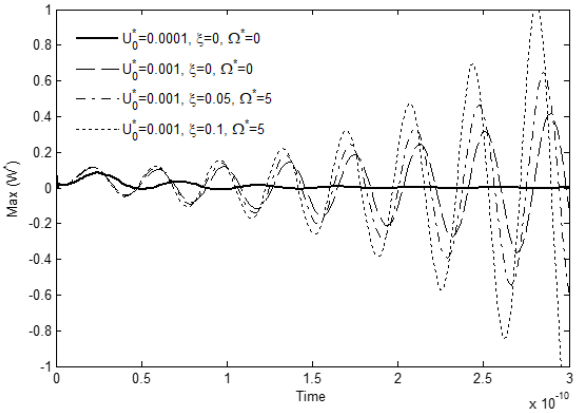

(b) Unstable condition $U_0^* > U_{fc}$

Fig. 13 Maximum amplitude of transverse displacement for various fluid flow velocities

5.3 Electro-thermo dynamical response analyses

The electro thermo dynamical responses of the smart micro shell are examined in Figs. 12 and 13 for various magnitudes of U_0^*, ξ and Ω^*. As can be seen from these figures by increasing both of U_0^* and ξ the frequency and the amplitudes of the response will be increased which is because of increasing the total energy level of the system due to increasing mean and pulsation amplitudes of flow velocity. In addition, comparing U_0^* and ξ it can be concluded that pulsation amplitude of the fluid flow regime play an important role on the instability of the system. In Figs. 11(a)-(b) and 12(a)-(b), the effect of stability is also considered when the flow velocity regime is under ($U_0^* = 0.001$) and over ($U_0^* = 0.0015$) the first mode critical flow velocity, respectively.

6. Conclusions

Instability prediction of a fluid conveying pipe (as a historical challenge for the engineers) in micro scale and with internal pulsating flow regime is investigated in this study. To obtain a stability active control of the system (sensing and actuating) the piezoelectric material is employed for the body and effects of applying external electric field on the stability of the system is investigated. Nonlocal piezoelasticity theory, nonlinear cylindrical shell model and energy approaches are employed to obtain the nonlinear electro statically coupled equations of motion. Using mode expansion analyses the equations of motion are discretized and solved via the state space problem. Consequently, the boundaries of the parametric resonance instability are achieved via the Bolitin's method. In the numerical results, effects of various parameters such as mean flow velocity, small scale parameter, applied voltage, fluid viscosity, Knudsen number and elastic foundation constants on dynamical stabilities of the system is studied. As a significant result it is shown that the imposed positive electric potential field along the micro-shell, increases natural frequency, critical flow velocity and also the stability of the structure and vice versa. In addition, it is observed that fluid viscosity and small-scale parameter have major effects on the critical flow velocity and the stability of the system. This work is presented to extend or complete the application of hydraulic sensors or actuators in advanced nano/micro electro-mechanical systems.

References

Alinia, M.M. and Ghannadpour, S. (2009), "Nonlinear analysis of pressure loaded FGM plates", *Compos. Struct.*, **88**(3), 354-359.

https://doi.org/10.1016/j.compstruct.2008.04.013.
Amabili, M. (2008), *Nonlinear Vibrations and Stability of Shells and Plates*, Cambridge University Press, Parma, Italy.
Arani, A.G., Shajari, A.R., Amir, S. and Atabakhshian, V. (2013a), "Nonlinear fluid-induced vibration and instability of an embedded piezoelectric polymeric microtube using nonlocal elasticity theory", *J. Mech. Eng. Sci*., **227**(12), 2870-2885. https://doi.org/10.1177/0954406213479094.
Arani, A.G., Shajari, A.R., Atabakhshian, V., Amir, S. and Loghman, A. (2013b), "Nonlinear dynamical response of embedded fluid-conveyed micro-tube reinforced by BNNTs", *Compos. Part B Eng*., **44**(1), 424-432. https://doi.org/10.1016/j.compositesb.2012.04.025.
Ashley, H. and Haviland, G. (1950), "Bending vibrations of a pipeline containing flowing fluid", *J. Appl. Mech*., **72**, 229-232.
Atabakhshian, V., Shoshtari, A.R. and Karimi, M. (2015), "Electro-thermal vibration of a smart coupled nanobeam system with an internal flow based on nonlocal elasticity theory", *Physica B Condens. Matter*, **456**, 375-382. https://doi.org/10.1016/j.physb.2014.08.043.
Azrar, A., Azrar, L. and Aljinaidi, A.A. (2015), "Numerical modeling of dynamic and parametric instabilities of single-walled carbon nanotubes conveying pulsating and viscous fluid", *Compos. Struct*., **125**(8), 127-143. https://doi.org/10.1016/j.compstruct.2015.01.044.
Bolotin, V.V. (1964), *The Dynamic Stability of Elastic Systems*, Holden-Day, San Francisco, USA.
Da, H.L., Wang, L., Qian, Q. and Ni, Q. (2014), "Vortex-induced vibrations of pipes conveying pulsating fluid", *Ocean Eng.*, **77**, 12-22. https://doi.org/10.1016/j.oceaneng.2013.12.006.
Dharap, P., Li, Z., Nagarajaiah, S. and Barrera, E.V. (2004), "Nanotube film based on single-wall carbon nanotubes for strain sensing", *Nanotechnology*, **15**(3), 379. https://doi.org/10.1088/0957-4484/15/3/026.
Ding, H.J. and Chen, W.Q. (2001), *Three Dimensional Problems of Piezoelasticity*, Nova Science, New York, USA.
Eringen, C. (1983), "On differential equations of nonlocal elasticity and solutions of screw dislocation and surface waves", *J. Appl. Phys*., **54**, 4703-4710. https://doi.org/10.1063/1.332803.
Fox, R.W., Pritchard, P.J. and McDonald, A.T. (2008), *Introduction to Fluid Mechanics*, Wiley, New York, USA.
Gao, J. and Xu, B. (2009), "Applications of nanomaterials inside cells", *Nano Today*, **4**(1), 37-51. https://doi.org/10.1016/j.nantod.2008.10.009.
Gu, J., Ma, T. and Menglan, D. (2016), "Effect of aspect ratio on the dynamic response of a fluid-conveying pipe using the Timoshenko beam model", *Ocean Eng.*, **114**, 185-191. https://doi.org/10.1016/j.oceaneng.2016.01.021.
IEEE Standard (1978), IEEE Standard on Piezoelectricity, IEEE, New York, USA.
Karniadakis, G., Beskok, A. and Aluru, N. (2005), *Micro Flows Nano Flows: Fundamentals and Simulation*, Springer-Verlag, USA.
Kamm, R.D. and Pedley, T.J. (1989), "Flow in collapsible tubes: A brief review", *J. Biomech. Eng*., **111,** 177-179. https://doi.org/10.1115/1.3168362.
Kong, J., Franklin, N.R., Zhou, C., Chapline, M.G., Peng, S., Cho, K. and Dai, H. (2000), "Nanotube molecular wires as chemical sensors", *Science*, **287**(5453), 622-625. https://doi.org/10.1126/science.287.5453.622.
Kuang, Y.D., He, X.Q., Chen, C.Y. and Li, G.Q. (2009), "Analysis of nonlinear vibrations of double-walled carbon nanotubes conveying fluid", *Int. J. Comput. Mater. Sci. Surf. Eng*., **45**, 875-880. https://doi.org/10.1016/j.commatsci.2008.12.007.
Kurylov, Y. and Amabili, M. (2010), "Polynomial versus trigonometric expansions for nonlinear vibrations of circular cylindrical shells with different boundary conditions", *J. Sound Vib*., **329**(9), 1435-1449. https://doi.org/10.1016/j.jsv.2009.10.038.
Liang, F. and Su, Y. (2013), "Stability analysis of a single-walled carbon nanotube conveying pulsating and viscous fluid with nonlocal effect", *Appl. Math. Model.*, **37**, 6821-6828. https://doi.org/10.1016/j.apm.2013.01.053.
Paidoussis, M.P. (1998), *Fluid-Structure Interactions: Slender Structures and Axial Flow Volume 1*, Academic Press, London, UK.
Paidoussis, M.P. (2003), *Fluid-Structure Interactions: Slender Structures and Axial Flow, Volume 2*, Academic press, London, UK.
Paidoussis, M.P., Misra, A.K. and Chan, S.P. (1985), "Dynamics and stability of coaxial cylindrical shells conveying viscous fluid", *J. Appl. Mech. Trans.*, **52**(2), 389-396. https://doi.org/10.1016/0022-460X(84)90319-5.
Panda, L.N. and Kar, R.C. (2008), "Nonlinear dynamics of a pipe conveying pulsating fluid with combination, principal parametric and internal resonances", **309**, 375-406. https://doi.org/10.1016/j.jsv.2007.05.023.
Pellicano, F. and Amabili, M. (2006), "Dynamic instability and chaos of empty and fluid-filled circular cylindrical shells under periodic axial loads", *J. Sound Vib*., **293**, 227-252. https://doi.org/10.1016/j.jsv.2005.09.032.
Rashidi, V., Mirdamadi, H.R. and Shirani, E. (2012), "A novel model for vibrations of nanotubes conveying nanoflow", *Comput. Mater. Sci*., **51**, 347-352. https://doi.org/10.1016/j.commatsci.2011.07.030.
Reddy, J.N. and Wang, C.M. (2004), "Dynamics of fluid conveying beams: Governing equations and finite element models", CORE Report No. 2004-03, *Centre for Offshore Research and Engineering National University of Singapore*, Singapore.
Sadeghi, M.H. and Karimi-Dona, M.H. (2011), "Dynamic behavior of a fluid conveying pipe subjected to a moving sprung mass: an FEM-state space approach", *Int. J. Press. Vessels Pip.* **88**(4), 123-131. https://doi.org/10.1016/j.ijpvp.2011.02.004.
Shokouhmand, H., Isfahani, A.H.M. and Shirani, E. (2010), "Friction and heat transfer coefficient in micro and nano channels filled with potous media for wide range of Knudsen number", *Int. Comm. Heat Mass Transfer*, **37**, 890-894. https://doi.org/10.1016/j.icheatmasstransfer.2010.04.008.
Tubaldi, E., Amabili, V. and Païdoussis, M.P. (2016), "Fluid-structure interaction for nonlinear response of shells conveying pulsatile flow", *J. Sound Vib*., **371**, 252-276. https://doi.org/10.1016/j.jsv.2016.01.024
Tubaldi, E., Amabili, M. and Paidoussis, M.P. (2017), "Nonlinear dynamics of shells conveying pulsatile flow with pulse-wave propagation: Theory and numerical results for a single harmonic pulsation", *J. Sound Vib*., **396**, 217-245. https://doi.org/10.1016/j.jsv.2017.01.044.
Wang, L. (2009), "A further study on the non-linear dynamics of simply supported pipes conveying pulsating fluid", *Int. J. Nonlinear Mech*., **44**, 115-121. https://doi.org/10.1016/j.ijnonlinmec.2008.08.010.
Yan, Y., Wang, W.Q. and Zhang, L.X. (2009), "Dynamical behaviors of fluid-conveyed multi walled carbon nanotubes", *Appl. Math. Model*., **33**, 1430-1440. https://doi.org/10.1016/j.apm.2008.02.010.
Yang, J. (2005), *An Introduction to the Theory of Piezoelectricity*, Springer, Lincoln, USA.
Yang, J., Ke, L.L. and Kitipornchai, S. (2010), "Nonlinear free vibration of single-walled carbon nanotubes using nonlocal Timoshenko beam theory", *Physica E Low Dimens. Syst. Nanostruct*., **42**, 1727-1735. https://doi.org/10.1016/j.physe.2010.01.035.
Yang, K.S., Cheng, Y.C., Liu, M.C. and Shyu, J.C. (2015), "Micro

pulsating heat pipes with alternate microchannel widths", *Appl. Therm. Eng.*, **83**, 131-138. https://doi.org/10.1016/j.applthermaleng.2015.03.020.

JL